Journal of Intelligent & Robotic Systems
https://doi.org/10.1007/s10846-019-01132-9

An Experimental Analysis on Propeller Performance in a Climate-controlled Facility

Matteo Scanavino[1] · **Andrea Vilardi**[2] · **Giorgio Guglieri**[1]

Received: 11 September 2019 / Accepted: 4 December 2019

Abstract

Despite many commercial applications make extensive use of Unmanned Aircraft Systems (UAS), there is still lack of published data about their performance under unconventional weather conditions. In the last years, multirotors and fixed wing vehicles, commonly referred to as drones, have been studied in wind environments so that stability and controllability have been improved. However, other important weather variables have impact on UAS performance and they should be properly investigated for a deeper understanding of such vehicles. The primary objective of our study is the preliminary characterization of a propeller in a climate-controlled chamber. Mechanical and electrical data have been measured while testing the propeller at low pressure and cold temperatures. Test results point out that thrust and electric power are strongly affected by air density. A comparison between the experimental data and the results of the Blade Element Theory is carried out to assess the theory capability to estimate thrust in unconventional environments. The overlap between experimental data and theory computation is appropriate despite geometrical uncertainties and corroborate the need of a reliable aerodynamic database. Propeller performance data under unconventional atmospheres will be leveraged to improve UAS design, propulsion system modelling as well as provide guidelines to certify operations in extreme environments.

Keywords Propeller performance · Unmanned aircraft system test bench · Harsh environmental coditions · Blade element theory

1 Introduction

In the last few years, multi-copter and fixed wing unmanned platforms have become popular vehicles for recreational and commercial applications. Low costs, high flexibility and new advanced flight modes allowed thousands of applications beyond the boundaries of conventional remote sensing scenarios. Unmanned Aircraft Systems (UAS) offer great potential in harsh environments (i.e. earthquakes, avalanches, and floods) and in the next future they will support and partially replace manned vehicles when dangerous missions are accomplished. The industry of small UAS heavily makes use of commercial-of-the-shelf (COTS) components to ensure low market prices. COTS usually experience higher failure rates than aeronautical products as predictable lifetime is not as important as in the aviation industry. In the analysis of one hundred drone events reported in [15], it is shown that the equipment problem is the third cause of UAS uncontrollability experienced by users. Moreover, in the context of Smart Cities, robotic aerial platforms will be extensively leveraged to provide services to citizens, e.g. collecting data for monitoring and security purposes. UAS management in cities requires an adequate Unmanned Traffic Management (UTM) system which can handle vehicle's trajectories without compromising safety. Critical information concerning the interaction between temperature as well as pressure and UAS power consumption, motor speed and propeller thrust will be mandatory for a safe management of unmanned aerial vehicles. A database on UAS performance in unconventional environments is still missing and will be a key element to evaluate battery lifetime and thrust prediction as

✉ Matteo Scanavino
matteo.scanavino@polito.it

[1] Department of Mechanical and Aerospace Engineering, Politecnico di Torino, Corso Duca degli Abruzzi 24, 10129, Torino, Italy

[2] terraXcube, Eurac Research, Via Ipazia 2, 39100, Bolzano, Italy

Published online: 10 January 2020

a function of weather for traffic management and failure rate purposes. The primary objective of our study is to provide a data set on propeller performance in low pressure and cold temperatures for a preliminary study on the effects of environmental conditions on UAS propulsion system.

In the past years some experimental activities have been carried out on small UAS and their power system. Brandt and Selig [6] focused on the characterization of propellers for small unmanned aerial platforms, providing a reference database to highlight thrust production and power consumption in wind environments. The investigation of propeller behaviour in low Reynolds flow conditions has been the target of their research. Another major contribute has been given by Russel [14] and performed at NASA Ames research centre. The authors have tested five commercial UAS in wind tunnel and static conditions, providing a complete database on overall performance of unmanned aerial vehicles. The major mechanical and electrical quantities, such as thrust, torques, motor speed, voltage and current, have been reported as a function of the wind tunnel speed and UAS attitude with respect to the airflow direction. The technical publication reports details on the experimental setup, test matrix, results and it is enriched by valuable data on propeller geometries obtained by laser scanner measurements. When considering UAS in harsh environments, few works describing vehicle performance are available. In 2016, PrecisionHawk [2] in collaboration with the Automotive Centre of Excellence at the University of Ontario, Canada, made environmental tests on multirotor and fixed wing platforms. However, experimental data have not been made available for research purposes. More recently, a relevant work has been published on propeller thrust generation in dynamic ice accretion conditions [10–12]. The experimental studies account for the aerodynamic performance of rotating blades in several water content and operating temperature conditions. The purpose of the characterization was the design of an innovative anti-ice propeller subsystem to avoid power consumptions. A passive solution based on surface wettability and hydrophobic materials has been proposed.

The activities previously described provide guidelines in the experimental testing of UAS, however, a lot of missing topics are still to be examined. A systematic approach on drone flight capabilities in high altitude flights, low temperature and high humidity has not been carried out by the academic research. Standard procedures for testing the propulsion system as well as the overall UAS are not defined in the industry either, resulting in unexploited vehicle capabilities. Moreover, a bias in the existing tests has been the non-reproducibility of the same climatic conditions. The experience reported by pilots when flying in specific atmospheres contribute to increase knowledge, but these efforts are not enough for a deep understanding of the phenomena. The UAS industry has recently started to give information to the end users concerning flight recommendations in unconventional environments. As an example, in the Alta 8 flight manual [7], by Freefly System, a table summarizing the maximum take-off weight as a function of temperature and altitude is provided. Data are based on predictions, real tests and user feedback beyond standard flight conditions.

For the aforementioned reasons, the primary objective of our study is to exploit a dedicated climate-controlled facility and carry out experimental data on small UAS propeller performance in low pressure and extreme temperatures. The environmental simulator is leveraged to provide a systematic approach on UAS vehicle performance and fill the gap in recent experimental research on multirotor and fixed wing aerial platforms. The broader goal of the research is to collect a set of data under unconventional weather conditions to improve propulsion system design and modelling for UAS applications. Power consumption performance as well as propeller thrust data will be useful for UAS traffic management purposes and improve the reliability of unmanned vehicles. This article is structured as follows. Section 2 describes the environmental facility employed in the experimental activity, reporting its main capabilities and limitations for UAS testing. Test details are reported in Section 3 providing information on the test bench, data acquisition system as well as the simulated atmospheres. Results for temperature and pressure tests at different motor speed are discussed in Section 4. A comparison between the experimental data and thrust predicted exploiting the Blade Element Theory (BET) is reported in Section 5. Finally, conclusions and future works are given in Section 6.

2 Environmental Simulator

The primary objective of this work is the preliminary characterization of a propeller in low pressure and cold temperatures when the UAS propulsion system is subjected to unconventional environments. The measurements took place inside *terraXcube*, an environmental simulator, in Bolzano, Italy, in collaboration with Eurac Research institute [4]. This *unique* facility has been designed for medical research on human physiology in extreme weathers. However, the laboratory is suitable for industrial tests, and has been exploited to carry out activities on UAS platforms.

The facility consists of two environmental hypobaric simulators: i) the main chamber (*large cube*) and, ii) four small independent simulators (*small cubes*). The experimental setup has been installed inside the main chamber (Figs. 1 and 2) to avoid aerodynamic interference with wall, ceiling and floor. The test section dimensions

Fig. 1 Experimental setup inside terraXcube main simulator for propeller testing

are 5 m x 12 m x 6 m (L x W x H respectively) and the test engineer can set temperatures (from −40°C to +60°C) and pressures (from sea level up to 300 hPa).

Fig. 2 Rotor assembly and schematic of thrust and airflow directions

Other features are available (e.g. humidity control, wind and precipitations) but have not been exploited because out of the scope of the tests. This simulator is not comparable to climatic wind tunnels because not designed for aerodynamic flow analysis. For this reason, the fan installed inside the chamber has never been turned on during the tests and all the measurements have been limited to static conditions (hover tests).

3 Technical Details of the Tests

A T-Motor 15′ x 5′ carbon fibre propeller (Fig. 3) has been tested due to its common employment in commercial and professional UAS, such as the SUI Endurance Aircraft. Furthermore, experimental data reported by the manufacturer datasheet [5] and by NASA Ames investigations [14] are available to make a comparison of the measurements in standard conditions. The rotor assembly, shown in Fig. 2, consisted of a T-Motor U5 KV 400 Brushless Direct Current (BLDC) motor managed by the T-Motor T60A electronic speed controller. The U5 is an out-runner brushless equipped with 14 magnetic poles mounted in the rotor case.

The assembly has been placed inside the chamber at the top of a support rod, secured to the floor to avoid displacements and designed to reduce mechanical vibrations. The equipment has been installed 1.5 m away from lateral wall, 2 m from the simulator main door and at 2 m height from the floor, as in Fig. 1. The propeller rotation axis has been aligned with the chamber main dimension to exploit all the available volume and prevent aerodynamic interference. The propeller has been combined with the BLDC direction of rotation to generate an airflow downstream the motor case and attenuate blockage effects (Fig. 2). Although this is not the conventional mounting, because motor and electronic speed controller are not immersed in the airflow, this configuration has been chosen to guarantee the lowest aerodynamic interaction between the propeller, motor case and test bench arm. As a result, during the tests, the load cell has always been compressed by the thrust generated by the propeller.

All the measurements have been taken using the RCbencmark 1520 test stand [3] which consists of: i) a 5 kgf load cell, ii) a precision shunt resistor for current sensing, iii) an electric probe for motor speed measurements and, iv) a circuit board to manage the interface between the electronic speed controller and a computer for control and logging purposes. The motor speed probe senses the electric current flowing in one of the BLDC phases, while a Fast-Fourier-Transform (FFT) algorithm computes the speed based on the number of magnetic poles placed in the rotor. According to the manufacturer, all the components are

Fig. 3 Top and lateral view of the T-Motor 15′ x 5′ carbon fibre propeller used for the tests

rated from −40°C to +85°C with storage down to −55°C and the load cell is temperature compensated. Although the test bed is not officially certified for such temperatures, preliminary tests have corroborated the capability of the load cell unit to work properly in the weather conditions of interest.

Figure 4 shows the overall architecture of the acquisition, control and power units. A dedicated power-supplier (22.5 V, 20 A) has been installed inside the control room to avoid testing downtime due to battery recharging. LiPo battery performance are strongly affected by temperature [13] and deep analysis on capacity, voltage and discharge rate for UAS applications will be conducted in the next future. The objective of this study is the evaluation of temperature and pressure on propeller aerodynamics without focusing on the chemistry of batteries. The test engineer has set different Pulse-Width-Modulation (PWM) signals to the electronic speed controller from a computer placed inside the control room. The same work station has been exploited for data recordings and monitoring during test execution. The data acquisition circuit board is part of the test bench equipment and has been placed inside the test section. The motor speed sensor, thrust load cell (strain gauge) as well as electric current and voltage sensors have been directly connected to the board.

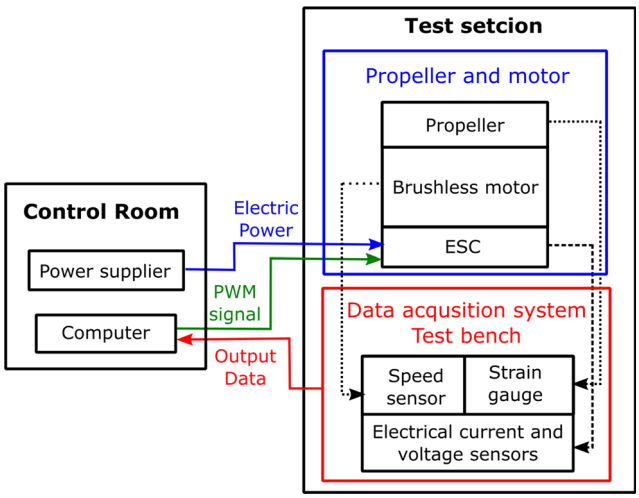

Fig. 4 Schematic of the data acquisition, control and power system for the tests

The RCBenchmark test bench is equipped with a set of pre-defined scripts to control the motor at different speeds. To standardize the measurement process, all the tests have been automate. When the desired environmental condition was reached inside the main chamber, the test engineer launched the script and monitored the process without worrying about the PWM control signals. The predefined scripts have been modified to execute a step sequence from the lowest to the highest value. The PWM considered are 1175 us, 1553 us, 1750 us and 1950 us respectively, as they envelop the normal operating signals for the rotor when installed on-board the UAS. The script sweeps between the lowest to highest input values. Each step consists of a settling time after which a new log measurement is taken. To reduce noise, the samples were averaged and then recorded. Finally, before any recordings, the stain gauge calibration process has been made to ensure goodness of the measurements.

3.1 Simulated Atmospheres

The environmental quantities considered are temperature and pressure independently. In the first use case, pressure is almost constant while temperature is set by the test engineer (isobaric test). In the second scenario, pressure is controlled while the temperature is almost constant (isothermal test). Details of the atmospheres replicated by tests are reported in Tables 1 and 2 for temperature and

Table 1 Atmospheric conditions for temperature tests

Temperature [°C]	Pressure [hPa]	Air density [kg/m^3]
42.5	989	1.0924
33.3	990	1.1256
29.3	990	1.1405
24.8	990	1.1577
18.1	983	1.1760
−13.5	978	1.3124
−20.3	978	1.3477
−25.7	978	1.3771
−28.4	977	1.3909
−34.5	974	1.4221

Table 2 Atmospheric conditions for pressure tests

Temperature [°C]	Pressure [hPa]	Air density [kg/m^3]	Altitude [m]
30.2	990	1.1371	206
29.8	943	1.0842	642
30.1	915	1.0509	910
29.9	884	1.0160	1215
30.4	867	0.9952	1385
30.2	855	0.9822	1507
29.8	842	0.9684	1641
30.0	807	0.9275	2019
30.0	796	0.9149	2141
17.9	541	0.6471	5353
21.0	299	0.3542	10053

pressure respectively. The equivalent altitude reported in Table 2 has been computed according to the barometric altitude equation:

$$z = -\log\left(\frac{p}{p_0}\right)\frac{R^* t}{g}, \tag{1}$$

where z is the altitude, p is the pressure, p_0 is the reference pressure, t is the temperature, R^* is the specific air constant and g is the gravitational acceleration. The air density ρ has been computed using the ideal gas law:

$$\rho = \frac{p}{R^* t}. \tag{2}$$

From Table 2, it can be noted the the last two pressure tests have been executed with slightly different temperatures. Air densities for the last two pressure tests are over-estimated by 4.07% and 2.96% respectively due to lower temperatures. These percentage variations do not compromise the tests as the phenomenon is dominated by pressure changes (45.35% and 69.80% pressure reduction).

Since the chamber was not fully tested and since it was not easy (at the project stage) to set in a straightforward way the variation intervals, we focused on extreme environmental conditions (extremely low temperature and pressure). A detailed investigation on the overall temperature and pressure range will be conducted in the next test campaign (2020), when the climatic chamber will be fully operational.

3.2 Measurements and Data Reduction

The data provided by the test bench circuit board are propeller thrust, motor speed, electric current and voltage (refer to Table 3). Based on the measurements, the following quantities can be computed

Table 3 Signals recorded by the data acquisition system

Symbol	Meaning	Unit	Note
I	BLDC current	A	Output
P	BLDC electric power	W	Output
Ω	Motor speed	rpm	Output
T	Propeller thrust	N	Output

$$\begin{aligned} c_T &= \frac{T}{\rho R^4 (\Omega)^2}, \\ c_P &= \frac{P}{\rho R^5 (\Omega)^3}, \\ R_e &= \frac{\rho \Omega (Rc)_{75\%}}{\mu}, \end{aligned} \tag{3}$$

where c_T is the thrust coefficient, T is the propeller thrust, R is the propeller radius, Ω is the motor angular speed in revolution per second, c_P is the power coefficient, P is the electric power required by the motor, R_e is the Reynolds number, c is the propeller chord and, μ is the air viscosity based on Sutherland's law as a function of temperature. The Reynolds number has been evaluated at 75% of the propeller radius. Percentage changes of thrust, motor speed and power have been computed with respect to the reference conditions as reported in the next paragraph. Thrust and power coefficients are given according to the standard definition for propeller as in [6].

4 Test Results

In this section, temperature and pressure test results are provided to the reader. It is important to remind that the environmental variables affect thrust and required mechanical power as a consequence of air density changes. Based on the disk actuator theory for stationary rotors, thrust and power equations are the followings

$$\begin{aligned} T &= 2\rho A v_i^2, \\ P &= \sqrt{\frac{T^3}{2\rho A}}, \end{aligned} \tag{4}$$

where A is the rotor disk area and v_i is the velocity of the air induced by the propeller at the rotor disk. As a result, thrust and power are directly proportional to the air density.

4.1 Temperature Test

Thrust and motor speed measurements are shown in Figs. 5 and 6 respectively. As the temperature decreases, thrust generated by the propeller increases as a direct consequence

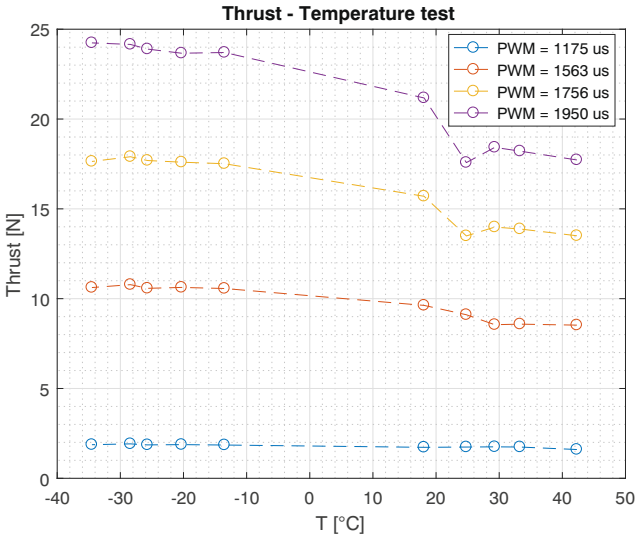

Fig. 5 Measured propeller thrust for temperature tests

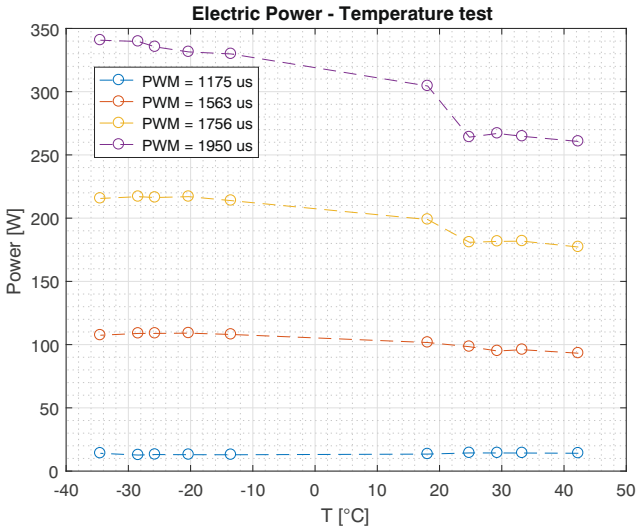

Fig. 7 Electric power for temperature tests

of higher air density. The motor speed is slightly affected by temperature and at constant PWM signal, the general trend is the lower the temperature, the slower the motor. The electric power, in Figs. 7, denotes a similar behaviour: as the temperature is reduced, the required power increases, owing to the higher mechanical work required to move the blades.

All the measurements have been compared to their value at 18.1°C, which is the closest value to standard air temperature conditions. Thrust and power percentage changes are shown in Figs. 8 and 9 respectively. At −34.5°C, thrust increase is almost between 10% and 15% according to the considered PWM signal. On the other side, at high temperature thrust and required power are reduced.

Comparing air density and thrust percentage changes, we found that thrust curve is lower than the expected air density percentage change when considering low temperature. The reason of this behaviour is related to non-constant motor speed despite the same PWM signals are set. Figure 10 corroborates that when temperature is reduced the motor angular speed is slower. As the air density increases, the propeller experiences higher lift and drag forces. Drag is responsible for torque and as a result, the lower the temperature, the higher the torque on the blades. At constant PWM signal, if the temperature is reduced then the motor spins slower, owing to the higher torque load.

The dotted blue curve in Figs. 8 and 9 are the computed thrust and power percentage changes combining air density and motor speed variations assuming constant thrust and power coefficients. The experimental data follow Eq. 5

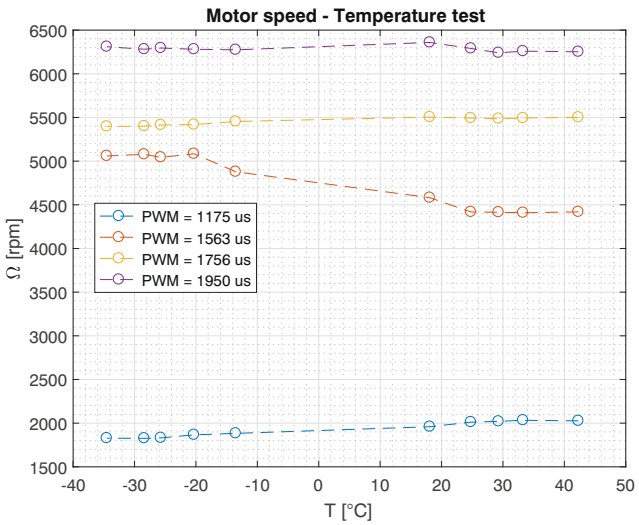

Fig. 6 Measured motor speed for temperature tests

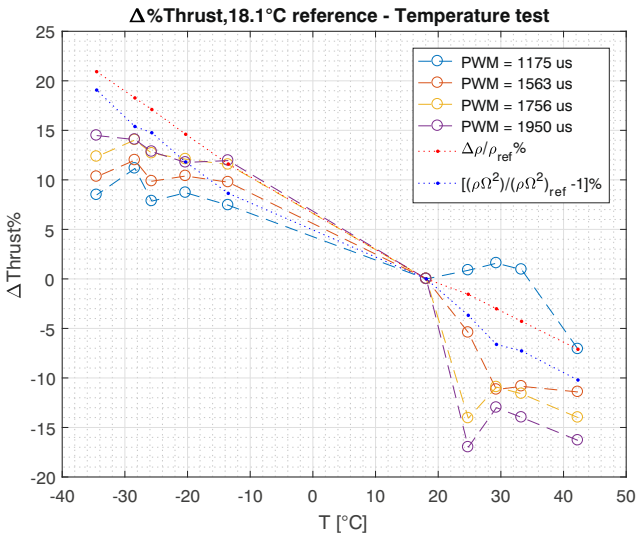

Fig. 8 Computed percentage change of propeller thrust for temperature tests

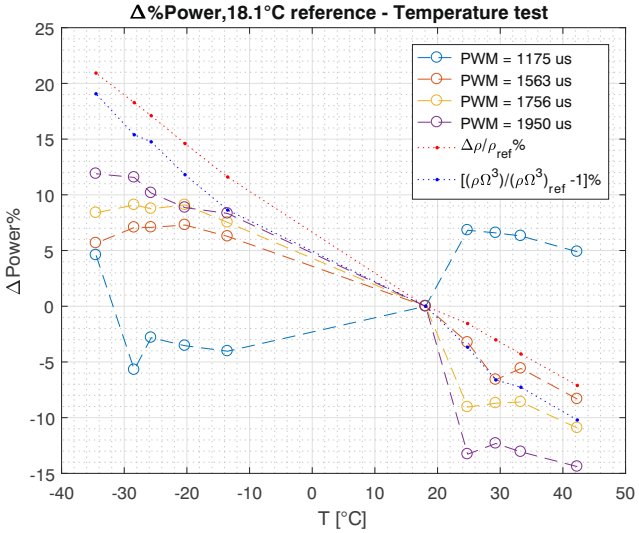

Fig. 9 Computed percentage change of electric power for temperature tests

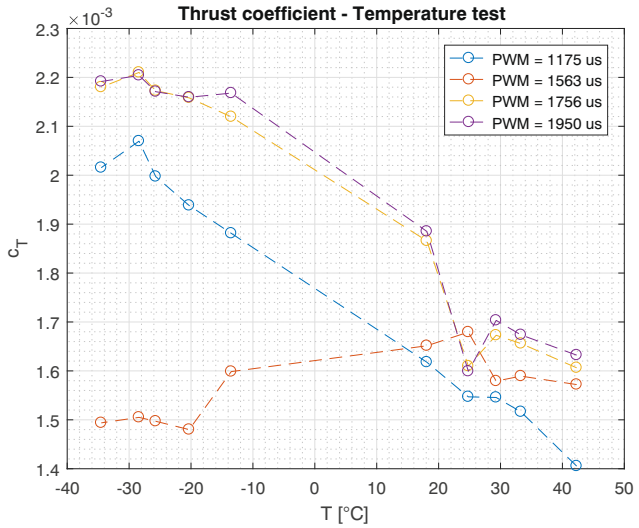

Fig. 11 Propeller thrust coefficient for temperature tests

rather than air density changes due to non-constant motor speed at constant PWM signal.

$$\Delta T\% = \left[\frac{\rho\Omega^2}{(\rho\Omega^2)_{ref}} - 1\right]\%,$$
$$\Delta P\% = \left[\frac{\rho\Omega^3}{(\rho\Omega^3)_{ref}} - 1\right]\%. \quad (5)$$

The motor speed percentage change corresponding to $PWM = 1563$ us does not follow the expected behaviour and could be related to inaccurate readings from the speed sensor. The same applies to power changes evaluated at $PWM = 1175$ us (Fig. 9): this curve is affected by inaccurate readings experienced from the shunt resistor, when small currents flow in the motor windings.

Thrust coefficient is reported in Fig. 11. The experimental data show a monotonically decreasing behaviour as the temperature is increased. The curve obtained at $PWM = 1563$ us is affected by inaccurate motor speed readings as already explained and is reported for completeness. The same trend can be evaluated for power coefficients: thrust and power coefficients are strongly affected by temperature inside the chamber. This is confirmed by the Reynolds number shown in Fig. 12: the lower the temperature, the less relevant the effects of air viscosity, the higher the thrust and power coefficients.

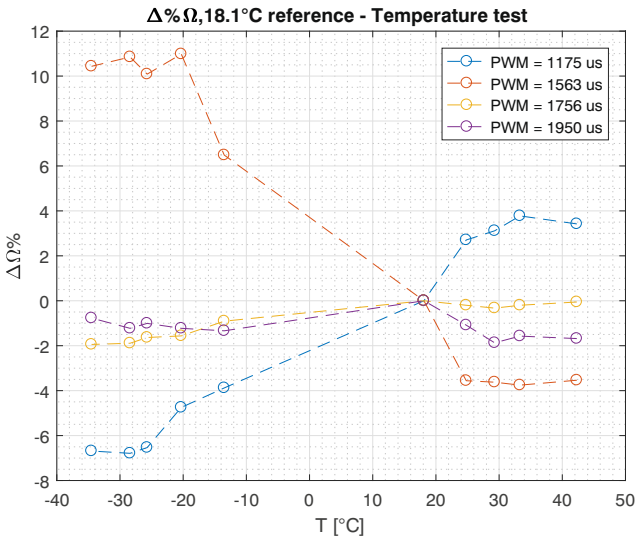

Fig. 10 Computed percentage change of BLDC motor speed for temperature tests

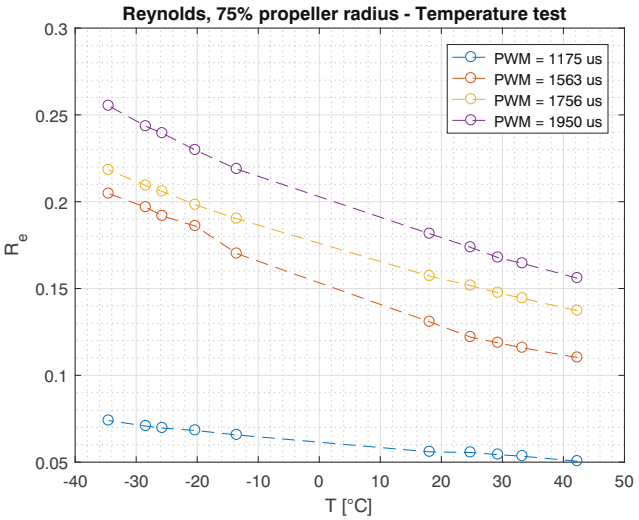

Fig. 12 Reynolds number evaluated at 75% for temperature tests

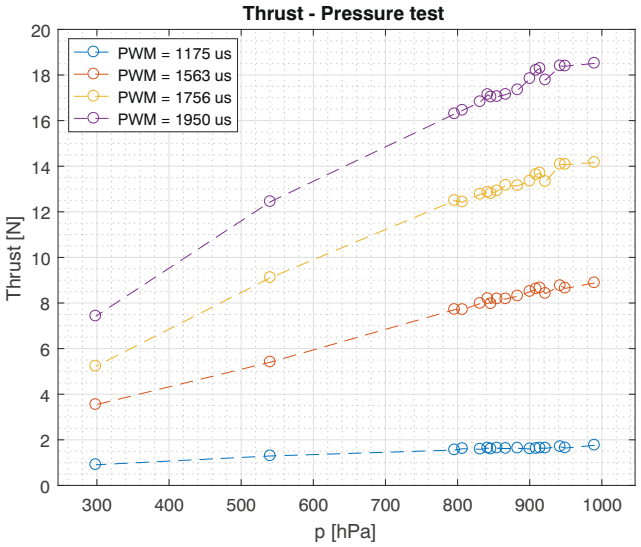

Fig. 13 Measured propeller thrust for pressure tests

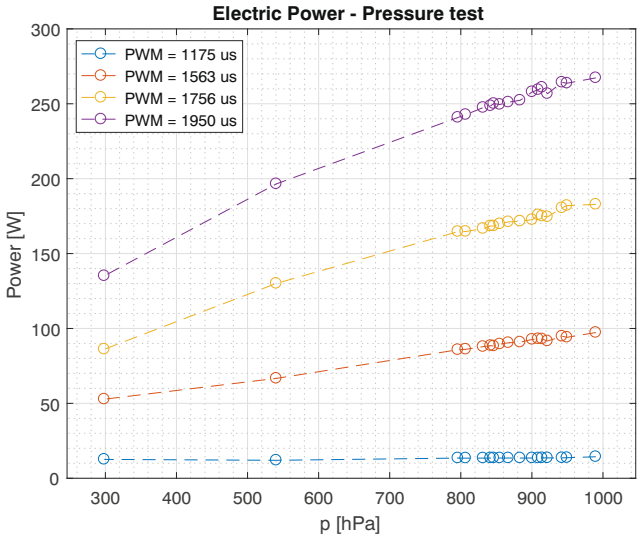

Fig. 15 Measured electric power for pressure tests. Electric current reveals a similar behaviour

4.2 Pressure Test

Thrust and motor speed as a function of pressure are reported in Figs. 13 and 14 respectively. Based on the ideal gas law in Eq. 2 at constant temperature, air density is directly proportional to pressure. For this reason, thrust shows a monotonically decreasing behaviour as the pressure is reduced. Given the same PWM signals, the required electric power (Fig. 15) and current are lower due to the smaller torques acting on the blades. While reducing the pressure, the motor spins faster as a consequence of the torque decrease. The aforementioned behaviour is clearly shown in Fig. 16: at the lowest pressure (highest simulated altitude in the chamber), the overall thrust reduction is closed to 60% (electric power is cut down by 50%). Thrust percentages are always greater than the air density curves. As for temperature tests, this behaviour is related to non-constant motor speed while working at constant PWM signals. The dotted blue curves in Fig. 16 are the computed percentage changes combining air density and motor speed assuming constant thrust coefficients. A good fit of the experimental data percentages is given by Eq. 5, as already reported for temperature tests. Thrust coefficients are given in Fig. 17. The computed values for high pressure are quite noisy; when extremely low pressure conditions are set, a reduction owing to the Reynolds number changes is clearly

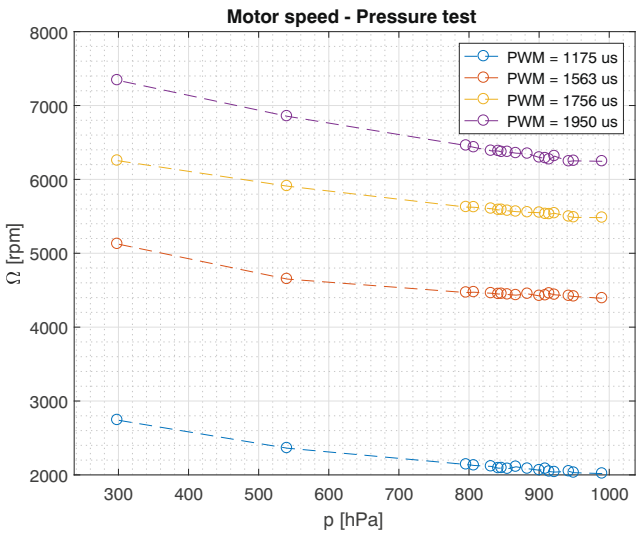

Fig. 14 Measured motor speed for pressure tests

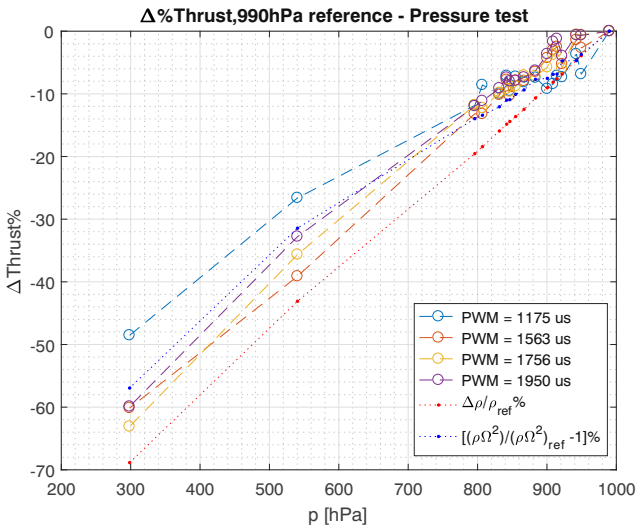

Fig. 16 Computed propeller thrust percentage change for pressure tests. Electric power experience the same trend

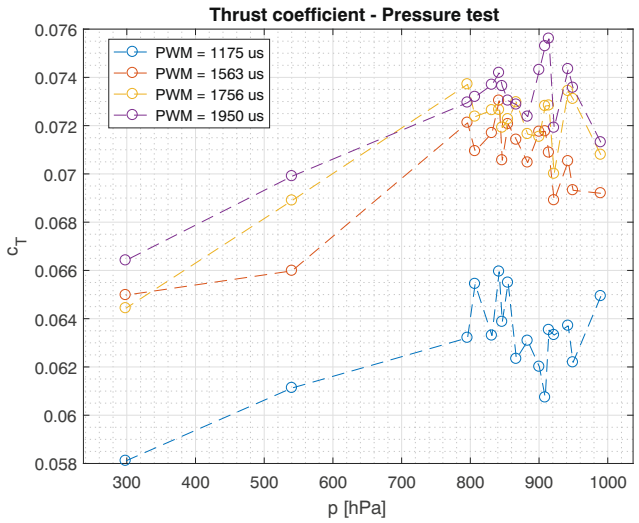

Fig. 17 Computed thrust coefficient for pressure tests

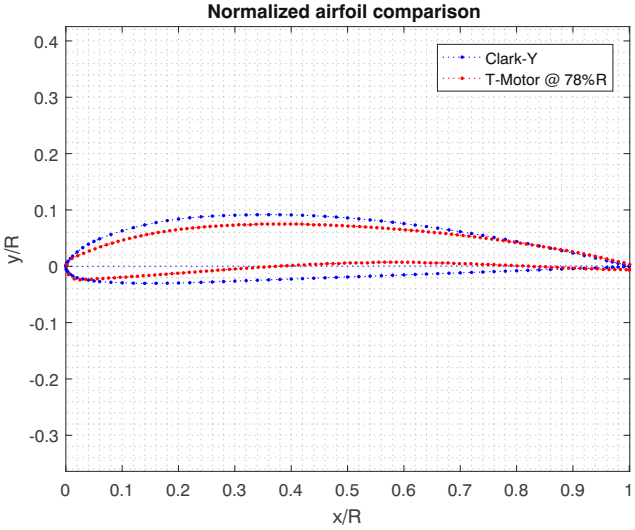

Fig. 19 Comparison between T-Motor profile at 75% of the propeller radius and Clark-Y airfoil

visible. As the altitude is increased (pressure reduced), the air viscosity effect becomes more relevant and the airflow conditions change as suggested by lower Reynolds numbers (Fig. 18).

5 Blade Element Theory Implementation

The Blade Element Theory (BET) allows to evaluate propeller performance given its geometrical characteristics, aerodynamic coefficients and operating environmental condition [1, 9]. Secondary effects, such as tip vortex and radial flow, are not considered by the theory. They usually have a negative impact on overall thrust generation; for these reasons, compared to experimental results, BET theory over-predict propeller thrust [1].

The geometry of the carbon-fibre T-Motor propeller is reported in [14]. Airfoil profile, chord and twist distributions are provided as a function of the distance from the propeller hub. As the propeller profile is not constant when moving along the radial direction, a simplified Clark-Y airfoil was used to perform all the computations. Figure 19 shows the T-Motor profile at 75% of the propeller radius compared with the Clark-Y airfoil. The maximum thickness and shape of the two profiles is a bit different. Although the choice of Clark-Y airfoil is a strong assumption, a detailed aerodynamic database as

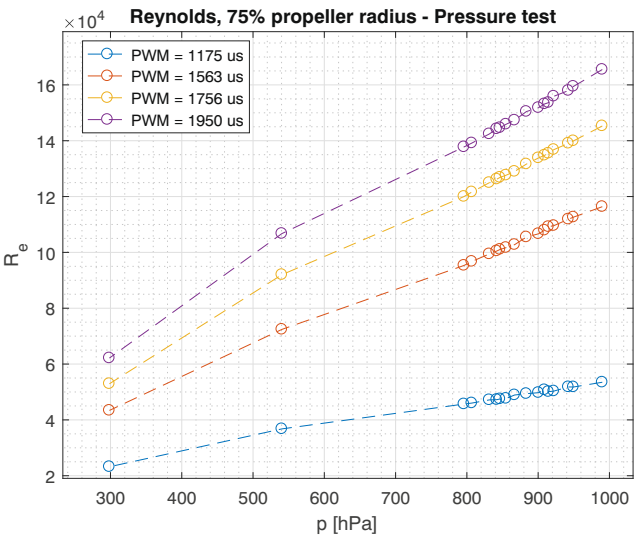

Fig. 18 Reynolds number computed at 75% of the propeller radius for pressure tests

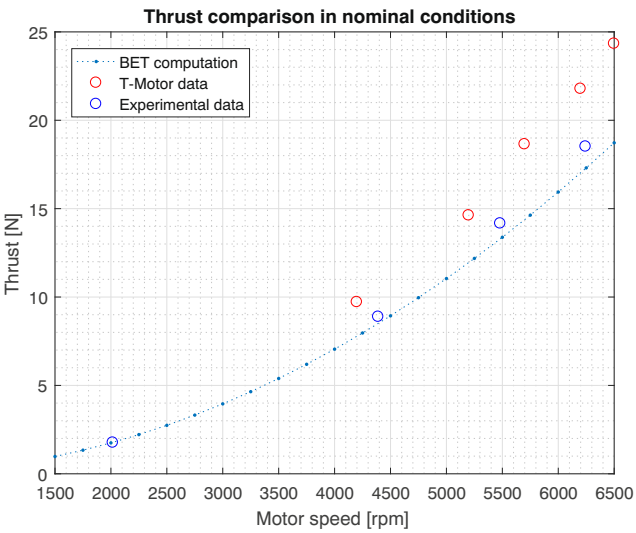

Fig. 20 Propeller thrust comparison between Blade Element Theory, T-Motor [5] and measurements collected inside terraXcube at 990 hPa and 30.2°C

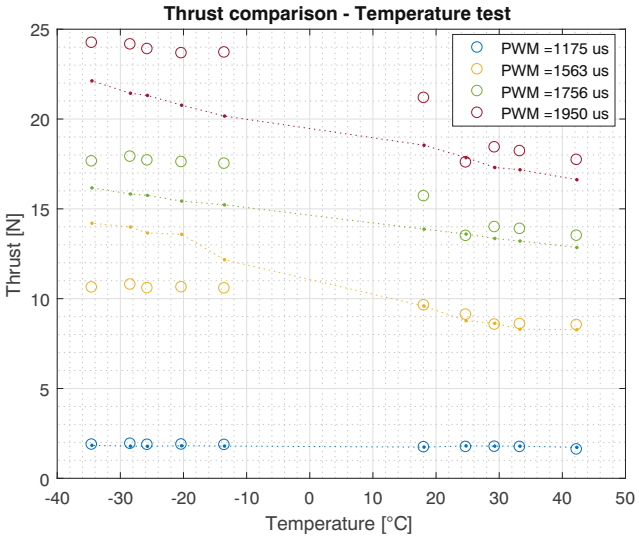

Fig. 21 Propeller thrust comparison between experimental data collected inside terraXcube and Blade Element Theory for temperature test. The dotted curves are the values computed using BET while the circle markers are the measurements of the tests

a function of angle of attack and Reynolds number was already available and validated for the Clark-Y [8]. This profile has been preferred to avoid the complexity of a CFD analysis for all the environmental conditions. The propeller has been divided in 100 elements ranging from 15% to 90% of the radius. These values have been chosen to avoid the root and tip contribution to thrust, due to BLDC motor interface and tip vortex respectively. Figure 20 compares propeller thrust evaluated by BET (dotted blue curve) with T-Motor specifications (red circles) [5] and experimental data (blue circles) in nominal conditions (990 hPa and 30.2°C). Despite the assumptions, BET results are closed to the measured data inside terraXcube than thrust values provided by the manufacturer.

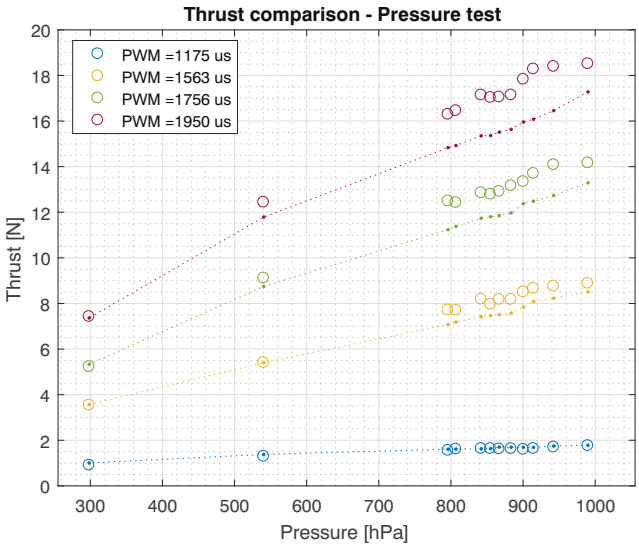

Fig. 22 Propeller thrust comparison between experimental data collected inside terraXcube and Blade Element Theory for pressure test. The dotted curves are the values computed using BET while the circle markers are the measurements of the tests

The experimental data provided in the previous section for temperature and pressure tests have been compared with the results of the blade element theory. The same climatic conditions (pressure and temperature) have been set for the computation. Moreover, the measured motor speed data for each PWM input signals has been used as input data in the BET implementation. Figures 21 and 22 compare measurements and BET for temperature and pressure tests. Details on percentage error between experimental results and BET are reported in Tables Appendix A and Appendix B.

The difference between the experimental data and the blade element theory is always lower than 15%, despite results obtained for temperature test at $PWM = 1563$ us enforcing the hypothesis of inaccurate readings from the motor speed sensor. Tables show that lower difference can be computed for pressure tests while higher difference are experienced for temperature tests highlighting the complexity of measurements in cold temperatures. Better results from the BET can be achieved using the real profiles instead of the Clark-Y assumption and a detailed aerodynamic database. The overall difference is reasonable for preliminary assessment and demonstrate that the BET is a suitable tool for propeller performance initial estimation.

All the experimental tests have been executed at constant PWM signal to avoid intervention on the electronic speed controller firmware and reduce the complexity of the software architecture. Future tests will take into account the need of motor speed feedback to allow the same angular rate while changing the environmental conditions. BET is exploited to obtain insights on thrust

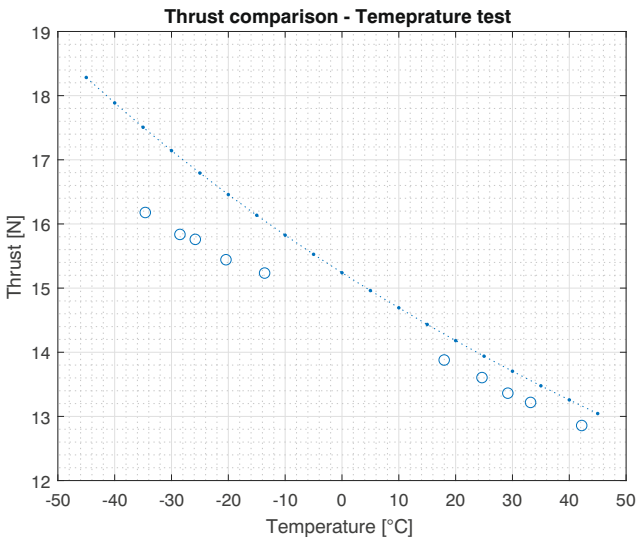

Fig. 23 Thrust computed at constant motor speed for temperature tests. Circles are the experimental data measured at constant PWM

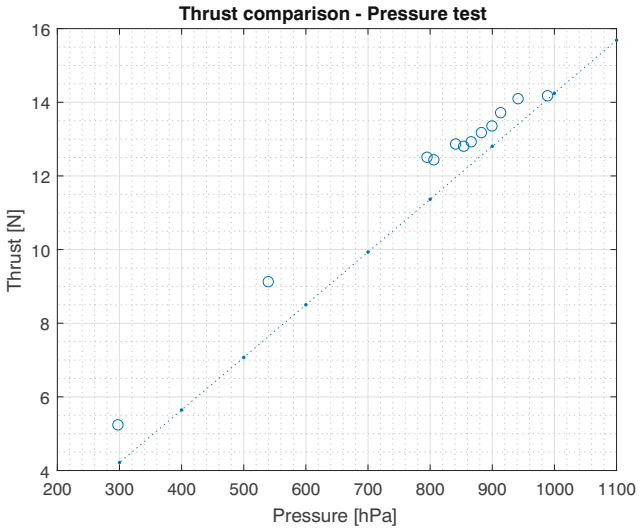

Fig. 24 Thrust computed at constant motor speed for pressure tests. Circles are the experimental data measured at constant PWM

production while working at constant motor speed for temperature and pressure tests. At constant pressure, thrust is inversely proportional to temperature (Fig. 23), while a direct proportional relationship is evident at constant temperature when pressure is changed (Fig. 24). The measured experimental data (blue circles) for $PWM = 1756$ us, which is the closest signal to the reference speed of 5500 rpm, highlight the effect of non-constant motor speed in the measurements taken during the experimental activity. For temperature tests, thrust increase is reduced by slower motor speed; while for pressure tests, thrust reduction is mitigated by motor speed increase.

6 Conclusions

This study present preliminary temperature and pressure test results on propeller performance in terms of thrust, motor speed, electric current and power since no environmental database is currently available for research purposes. The experimental activity has been carried on a propeller commonly used in UAS applications.

Results show that performances are greatly influenced by the operating environment. Higher thrust and electric power required by the brushless motor are measured as a consequence of cold temperatures. Low pressure tests highlight thrust and power reduction as the air density decreases. All the tests have been performed at constant PWM signals and a secondary effect has been observed: temperature and pressure are responsible for torque loading on the propeller, resulting in non-constant motor speed. Pressure and temperature changes have a direct effect on the aerodynamic coefficients as the Reynolds number varies according to the operating environmental conditions. The main limitation of the tests is related to inaccurate readings from speed and current sensor especially when low temperatures have been set.

The experimental data have been compared with results provided by the Blade Element Theory showing a good overlap even tough a Clark-Y airfoil has been adopted instead of the real profile distribution. The BET still remain an important tool for preliminary assessment when the propeller geometry is available. Environmental testing is mandatory to account for complex aerodynamic phenomena (e.g. rotor to rotor interaction, tip vortex loss) which are not considered by this simplified theory.

Future works include a more accurate experimental setup, the investigation of combined effects of temperature, pressure and humidity on propeller and complete UAS performance. The final goal is to collect a high quality set of data of unmanned vehicles performance in unconventional atmospheres. Second order effects, such as temperature influence on batteries and BLDC heat dissipation, will be examined for fine modelling of the propulsion system. The experimental activity will be leveraged to answer some of the open questions related to safety of operations in harsh weather conditions. Tests on complete UAS have been scheduled to develop test protocol standards and make progress on design of UAS involved in severe environments.

Acknowledgements The research leading to these results has received funding from the European Regional Development Fund 2014-2020 of , under Grant Agreement 2223/2017/Project number FESR1048, Creazione di un servizio di sviluppo tecnico per droni testati per il funzionamento in condizioni ambientali estreme, DronEx.

Appendix A: Propeller thrust experimental data and BET, temperature test

Table 4 Data for PWM = 1175 us

t [°C]	Ω [RPM]	Experimental [N]	BET [N]	$\Delta T\%$
42.3	2026	1.602	1.723	−7.534
33.3	2033	1.741	1.789	−2.757
29.3	2020	1.752	1.790	−2.175
24.8	2012	1.740	1.804	−3.661
18.1	1959	1.725	1.737	−0.684
−13.5	1883	1.853	1.794	3.184
−20.3	1866	1.875	1.810	3.472
−25.7	1831	1.860	1.781	4.247
−28.4	1826	1.917	1.789	6.667
−34.5	1828	1.871	1.834	1.962

Table 5 Data for PWM = 1563 us

t [°C]	Ω [RPM]	Experimental [N]	BET [N]	$\Delta T\%$
42.3	4419	8.527	8.271	2.999
33.3	4409	8.582	8.298	3.310
29.3	4415	8.550	8.626	−0.892
24.8	4418	9.105	8.772	3.654
18.1	4581	9.626	9.586	0.417
−13.5	4878	10.570	12.168	−15.114
−20.3	5084	10.630	13.582	−27.771
−25.7	5043	10.580	13.658	−29.095
−28.4	5078	10.780	13.990	−29.774
−34.5	5059	10.620	14.200	−33.711

Table 6 Data for PWM = 1756 us

t [°C]	Ω [RPM]	Experimental [N]	BET [N]	$\Delta T\%$
42.3	5501	13.500	12.848	4.830
33.3	5493	13.880	13.208	4.842
29.3	5486	13.980	13.352	4.491
24.8	5493	13.490	13.595	−0.778
18.1	5504	15.700	13.869	11.664
−13.5	5454	17.510	15.224	13.054
−20.3	5418	17.600	15.432	12.318
−25.7	5414	17.690	15.749	10.970
−28.4	5400	17.900	15.827	11.583
−34.5	5397	17.640	16.168	8.344

Table 7 Data for PWM = 1950

t [°C]	Ω [RPM]	Experimental [N]	BET [N]	$\Delta T\%$
42.3	6252	17.720	16.622	6.198
33.3	6259	18.210	17.176	5.677
29.3	6240	18.420	17.302	6.068
24.8	6290	17.580	17.855	−1.563
18.1	6359	21.170	18.540	12.423
−13.5	6274	23.700	20.166	14.913
−20.3	6281	23.660	20.770	12.216
−25.7	6295	23.890	21.314	10.782
−28.4	6281	24.150	21.435	11.244
−34.5	6310	24.240	22.125	8.726

Appendix B: Propeller thrust experimental data and BET, pressure test

Table 8 Data for PWM = 1175 us

$p\ [hPa]$	Ω [RPM]	Experimental [N]	BET [N]	$\Delta T\%$
990.0	2018	1.760	1.781	−1.193
942.5	2048	1.696	1.748	−3.072
914.5	2045	1.634	1.689	−3.341
900.5	2063	1.598	1.691	−5.845
883.5	2084	1.629	1.695	−4.052
867.0	2110	1.617	1.702	−5.238
855.0	2082	1.632	1.635	−0.153
842.0	2091	1.634	1.625	0.532
807.0	2128	1.609	1.611	−0.155
796.0	2141	1.552	1.609	−3.666
540.5	2362	1.292	1.379	−6.726
298.5	2742	0.906	1.005	−10.964

Table 9 Data for PWM = 1563 us

$p\ [hPa]$	Ω [RPM]	Experimental [N]	BET [N]	$\Delta T\%$
990.0	4391	8.880	8.506	4.207
942.5	4423	8.755	8.226	6.041
914.5	4456	8.657	8.091	6.538
900.5	4423	8.499	7.845	7.693
883.5	4433	8.175	7.579	7.297
867.0	4442	8.175	7.509	8.144
855.0	4451	7.964	7.471	6.193
842.0	4448	8.191	7.423	9.379
807.0	4473	7.706	7.187	6.738
796.0	4468	7.710	7.072	8.270
540.5	4651	5.406	5.406	1.074
298.5	5126	3.539	3.569	−0.848

Table 10 Data for PWM = 1756 us

$p\ [hPa]$	Ω [RPM]	Experimental [N]	BET [N]	$\Delta T\%$
990.0	5482	14.160	13.292	6.130
942.5	5497	14.080	12.736	9.543
914.5	5529	13.700	12.486	8.865
900.5	5550	13.340	12.383	7.177
883.5	5564	13.160	11.968	9.061
867.0	5575	12.910	11.857	8.159
855.0	5588	12.790	11.803	7.714
842.0	5587	12.850	11.739	8.644
807.0	5623	12.420	11.384	8.338
796.0	5625	12.490	11.236	10.038
540.5	5909	9.111	8.747	3.991
298.5	6254	5.224	5.331	−2.054

Table 11 Data for PWM = 1950 us

$p\ [hPa]$	Ω [RPM]	Experimental [N]	BET [N]	$\Delta T\%$
990.0	6245	18.510	17.278	6.659
942.5	6244	18.390	16.459	10.500
914.5	6270	18.280	16.081	12.028
900.5	6296	17.830	15.960	10.490
883.5	6355	17.140	15.637	8.770
867.0	6372	17.050	15.514	9.012
855.0	6371	17.030	15.367	9.768
842.0	6384	17.140	15.351	10.437
807.0	6434	16.450	14.928	9.255
796.0	6458	16.290	14.833	8.944
540.5	6855	12.440	11.790	5.227
298.5	7342	7.422	7.364	0.783

References

1. Blade element theory for propeller. http://www.aerodynamics4students.com/propulsion/blade-element-propeller-theory.php. Accessed: 2019-07-12
2. Precisionhawk explores extreme-weather testing of drones with ace research centre. https://www.precisionhawk.com/blog/media/topic/precisionhawk-explores-extreme-weather-testing-of-drones-with-ace-research-centre. Accessed: 2019-07-26
3. Series 1520 thrust stand - rcbenchmark. https://www.rcbenchmark.com/pages/series-1520. Accessed: 2019-07-26
4. terraxcube. https://terraxcube.eurac.edu/. Accessed: 2019-07-26
5. U5 t-motor propulsion system specifications. http://store-en.tmotor.com/goods.php?id=318. Accessed: 2019-07-09
6. Brandt, J., Selig, M.: Propeller Performance Data at Low Reynolds Numbers. In: 49Th AIAA Aerospace Sciences Meeting including the New Horizons Forum and Aerospace Exposition, p. 1255 (2011)
7. FreeflySystem: Alta 8 Aircraft Fligth Manual
8. Guglieri, G.: Effect of autopilot modes on flight performances of electric mini-uavs. Aeronaut. J **117**(1187), 57–69 (2013)
9. Houghton, E.L., Carpenter, P.W.: Aerodynamics for engineering students. Elsevier (2003)
10. Liu, Y., Li, L., Chen, W., Tian, W., Hu, H.: An experimental study on the aerodynamic performance degradation of a uas propeller model induced by ice accretion process. Exp. Thermal Fluid Sci. **102**, 101–112 (2019)
11. Liu, Y., Li, L., Li, H., Hu, H.: An experimental study of surface wettability effects on dynamic ice accretion process over an uas propeller model. Aerosp. Sci. Technol. **73**, 164–172 (2018)
12. Liu, Y., Li, L., Ning, Z., Tian, W., Hu, H.: Experimental investigation on the dynamic icing process over a rotating propeller model. J. Propuls. Power **34**(4), 933–946 (2018)
13. Navarathinam, N., Lee, R., Chesser, H.: Characterization of lithium-polymer batteries for cubesat applications. Acta Astronaut. **68**(11-12), 1752–1760 (2011)
14. Russell, C.R., Jung, J., Willink, G., Glasner, B.: Wind tunnel and hover performance test results for multicopter uas vehicles (2016)
15. Wild, G., Murray, J., Baxter, G.: Exploring civil drone accidents and incidents to help prevent potential air disasters. Aerospace **3**(3), 22 (2016)

Matteo Scanavino is currently a Ph.D. student in Aerospace Engineering at the Politecnico di Torino, Italy. He received his B.S. and M.S. in Aerospace Engineering from Politecnico di Torino in 2014 and 2016, respectively. His research interests include autonomous indoor navigation, autopilot development and implementation as well as performance analysis of unmanned aerial vehicles.

Andrea Vilardi PhD in Cognitive and Brain Science, is senior researcher and responsible for project development at terraXcube, Eurac Research, Bolzano, Italy.

Giorgio Guglieri is currently a Full Professor of Politecnico di Torino, Italy, in the Department of Mechanical and Aerospace Engineering. He received his M.S. degrees from Politecnico di Torino in 1989. His research interests include flight mechanics, unmanned aerial vehicles and space systems. He is a Senior Member of AIAA and a Member of AHS.